

## Hydrothermal Synthesis of TiO<sub>2</sub>(B) Nanowires/CNTs as Anode Material for High Performance Lithium-ion Batteries

Rong Jiang, Xiaoxiao Luo, Xiaogang Wen\*

School of Materials Science and Engineering, Sichuan University, Chengdu 610065, P. R. China

\*E-mail: [wengxg@scu.edu.cn](mailto:wengxg@scu.edu.cn)

Received: 10 July 2016 / Accepted: 31 August 2016 / Published: 10 October 2016

---

A novel TiO<sub>2</sub>(B) nanowires/carbon nanotubes (TNWs/CNTs) nanocomposite was designed and obtained via a simple hydrothermal reaction. The nanocomposites exhibit unique feature of TiO<sub>2</sub>(B) nanowires twined with CNTs. The addition of CNTs can increase the electrolyte/electrode contact area and improve the electrical conductivity. Comparing with pure TNWs, the TNWs/CNTs nanocomposites have greatly improved rate capability, it demonstrate high capacity of 355.9, 291.4, 263.8, 235.7 and 191.3 mAh.g<sup>-1</sup>, at current rate of 0.2, 0.5, 1, 2 and 5 C, respectively, and the capacity retention ratio is up to 90%. The results suggest the unique nanostructure and highly conductive carbon nanotubes induce excellent electrochemical performance of TNWs/CNTs nanocomposites, and make it a promising anode candidate for lithium-ion batteries (LIBs).

---

**Keywords:** TiO<sub>2</sub>(B) nanowires; Carbon nanotubes; Hydrothermal synthesis; Lithium ion batteries.

### 1. INTRODUCTION

Current concern about ever-growing energy consumption, coupled with the voice to decrease greenhouse gas emissions, has intensified research on renewable energies [1]. Lithium ion batteries (LIBs) have attracted much attention as power sources for portable electronic devices with many outstanding features including high energy density, capacity retention, long cycle life, low maintenance and environmental benignity [2-6]. However, LIBs still exist many limitations, such as capacity degradation and security issues during prolonged cycling [7]. It is still a challenge to solve these problems.

Recently, metal oxides have attracted intensive research interests because of their distinct lithium storage mechanisms and characteristics. Among the transition-metal oxides, nanostructured TiO<sub>2</sub> has been recognized as an alternative anode material for LIBs due to its high rate performance,

stable capacity retention, low cost, abundance and non-toxicity [8-13]. Anatase [8,12] and rutile [4,14] TiO<sub>2</sub> nanomaterials have been studied extensively. However, TiO<sub>2</sub> confronts the problem of poor electrical conductivity and low Li-ion diffusivity, which affect its LIBs performance. Therefore, it is highly desirable to develop reliable strategies to advance electrical conductivity and Li<sup>+</sup> diffusivity in TiO<sub>2</sub> [15,16]. Normally, nanostructured TiO<sub>2</sub> [7,8] can provide a higher electrode/electrolyte contact area, resulting in the significant improvement of insertion/extraction, the mesoporous TiO<sub>2</sub> [10-12] have also been synthesized to improve the electrical conductivity and Li<sup>+</sup> diffusivity in TiO<sub>2</sub>. On the other hand, various carbon-modified TiO<sub>2</sub> nanocomposites including carbon nanotube–TiO<sub>2</sub> nanoparticles [17], TiO<sub>2</sub>@carbon nanofibers [18], TiO<sub>2</sub>/C nanospheres [19] and TiO<sub>2</sub>–graphene–carbon nanotube nanocomposites [20] have been exploited in order to improve the electrical conductivity of TiO<sub>2</sub> nanostructures.

TiO<sub>2</sub>(B) as a minor crystal phase of TiO<sub>2</sub> (monoclinic), is different from anatase, rutile and brookite. Its nanostructures have been successfully synthesized and applied in photocatalytic hydrogen evolution [21], visible-light photoactivity[22], medical application [23]. Recently, the TiO<sub>2</sub>(B) nanomaterials including flower-like nanostructures [24], nanotubes coated with carbon [25], nanoribbons [26] and mesoporous microspheres [27] have been used as anode of LIBs and demonstrated improved performance. However, the TiO<sub>2</sub>(B) also confront the problems of poor electrical conductivity and low Li-ion diffusivity. In this paper, we designed and synthesized a novel TiO<sub>2</sub>(B) nanowires/CNTs nanocomposites. To our knowledge, this nanocomposites have not been reported yet. The addition of CNTs can increase the electrolyte/electrode contact area and improve the electrical conductivity. As well as combining the advantages of TiO<sub>2</sub>(B) nanowires and CNTs, this structure facilitates the transportation of the electrolyte ion and electron into the inner region of the electrode, which is beneficial for lithium-ion insertion/extraction and improve LIBs performance of the material.

## 2. EXPERIMENTAL SECTION

### 2.1. Materials and Synthesis

All chemical reagents including tetrabutyl titanate (TBT), deionized water (H<sub>2</sub>O), sodium hydroxide (NaOH), acetic acid (HAc), ethylene glycol (CH<sub>2</sub>OH)<sub>2</sub>, ethanol (C<sub>2</sub>H<sub>5</sub>OH), hydrochloric acid (HCl), nitric acid (HNO<sub>3</sub>) and sulfuric acid (H<sub>2</sub>SO<sub>4</sub>) (Chengdu Kelong Chemical Reagent Co., Ltd.) were of analytical grade and used without further purification.

CNTs (Chengdu Organic Chemical Co., Ltd.) were treated in the mixture of nitric acid and sulfuric acid (V: V = 1:3) for 24 h at room temperature before use. The TNWs/CNTs nanocomposites were synthesized by a hydrothermal method as follows: At first, 20 ml of (CH<sub>2</sub>OH)<sub>2</sub> and 3 ml of HAc were well mixed, and then a certain amount of CNTs and 6 ml of TBT were added; after being well mixed, 30 ml of NaOH (15 mol/L) were added, after being further stirred for 10 min, the mixture was transferred into a teflon-lined autoclave with a volume capacity of 100 mL. The autoclave was sealed and maintained at 180 °C for 24 h, and then cooled naturally to room temperature. The precipitate was

carefully collected by centrifugation and washed several times with distilled water and ethanol respectively, and then the precipitate was rinsed with HCl (0.1 mol/L) and dried in a vacuum oven at 80 °C for 12 h. Finally, the powder was placed in a muffle furnace and maintained at 350 °C for 2.5 h to obtain a black product for following characterization and measurement. As a comparison, the pure TiO<sub>2</sub>(B) nanowires were synthesized by the same process in the absence of CNTs.

## 2.2. Characterization

The morphological features of the samples were characterized by a scanning electron microscope (SEM, S-3400N), and transmission electron microscope (TEM) imaging was carried on a Tecnai G2F20 S-TWIN scanning TEM with selected area electron diffraction (SAED). All the X-ray diffraction (XRD) patterns were conducted on a X'Pert Pro MPD /max-B diffractometer using Cu K<sub>α</sub> radiation at a scanning rate of 5°/min in the range of 10–80°. Raman spectra were recorded at ambient temperature with a LabRAM HR Raman spectrometer.

## 2.3. Electrochemical Measurements

The electrochemical performance of synthesized samples were evaluated using CR2032 type coin cells. To fabricate the electrodes, the prepared samples were mixed with polyvinylidene fluoride (PVDF) binder and acetylene black (AB) at a weight ratio of 8:1:1 using N-methylpyrrolidone (NMP) as solvent. Then the resulting slurry was evenly cast onto a copper foil with thickness of 14 μm. After drying in air overnight, the electrodes were punched into wafers with diameters of 14 mm. The coin cells were assembled in an argon-filled glove box using the active material as the working electrode, a Li foil as the reference and counter electrode, a Celgard 2400 film as the separator, and a mixture of 1 mol/L LiPF<sub>6</sub> in ethylene carbonate and dimethyl carbonate (with a volume ratio of 1:1) as electrolyte. The galvanostatic charge/discharge tests were carried out at constant cut-off voltages of 1–3V at different current densities using a neware BTS-5V/50mA system (ShenZhen, China), charge/discharge tests were carried out at room temperature (20 °C). All the capacities and C-rate currents were calculated based on the total weight of TNWs/CNTs composite in the electrodes.

## 3. RESULTS AND DISCUSSION

As shown in Fig. 1, the morphology and microstructure of the product were investigated using SEM, TEM and SAED. Fig. 1a shows the SEM image of TNWs/CNTS nanocomposites, it can be seen that CNTs are dispersive and twine around the TNWs, this microstructure facilitate to improve the conductivity of the nanocomposites. As a comparison, Fig. 1b shows the SEM image of pure TNWs that synthesized in the absence of carbon nanotube. To further examine the architecture of the nanocomposites, the samples were investigated by TEM. Fig. 1c presents a typical TEM image of the TNWs/CNTs nanocomposites, in which flexible CNTs twine around rigid TNWs with an average

diameter of 30 nm. The measured interplanar spacing from HRTEM image (Fig. 1d) is about 2.04 Å, which matches well with (60-1) crystal face of TiO<sub>2</sub>(B), indicating the rigid nanowires are TiO<sub>2</sub>(B). The inset in Fig. 1d is the SAED pattern of TNWs, the diffraction rings states clearly the polycrystalline characteristics of the nanowires, and the several diffraction rings can be attributed to (200), (110) and (60-1) crystal face of TiO<sub>2</sub>(B), respectively. The amorphous CNTs can also be observed in the Fig. 1d, it confirms that products are TNWs/CNTs nanocomposites.

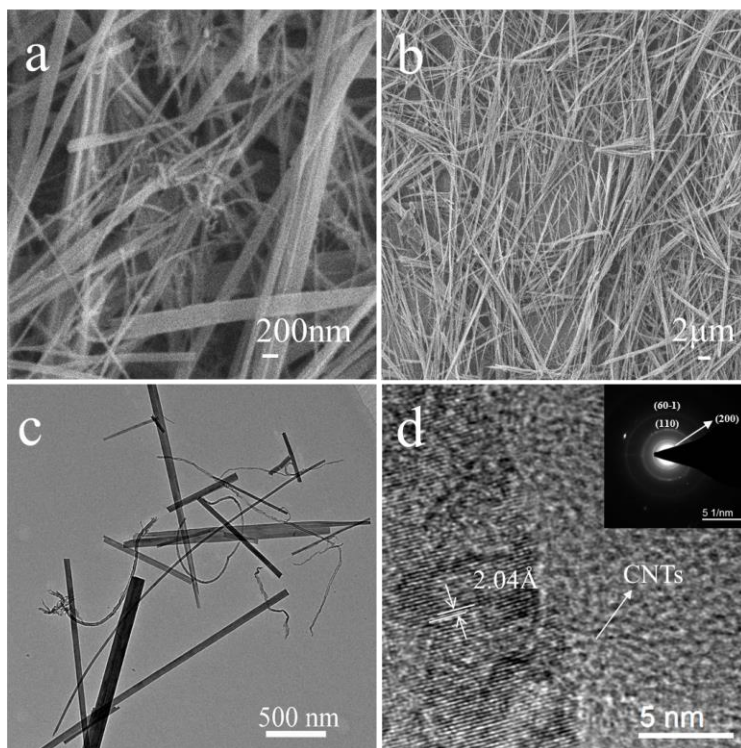


**Figure 1.** SEM, TEM, HRTEM images of samples. (a) SEM image of TNWs/CNTs, (b) SEM image of pure TNWs, (c) TEM of TNWs/CNTs and (d) HRTEM images of TNWs/CNTs. Inset in (d), SAED pattern of TNWs/CNTs.

In order to identify the composition of the products, the samples were characterized by XRD. Fig. 2a shows the XRD patterns of TNWs/CNTs and pure TNWs. For pure TNWs, the diffraction peaks match the TiO<sub>2</sub>(B) (JCPDS card No. 46-1237) well, after the addition of CNTs, no new peak appears in the XRD pattern, it indicates that the CNTs are amorphous.

The phase compositions of the as-obtained samples are further studied by raman. As shown in Fig. 2b, for both pure TNWs and TNWs/CNTs samples, the observed peaks at 123, 144.3, 197, 249.6, 409, 433.6, 469.8 and 634.2 cm<sup>-1</sup>, correspond to the characteristic peaks of TiO<sub>2</sub>(B) [25,26,]. After adding CNTs, two new peaks at 1349.1 and 1595.7 cm<sup>-1</sup> appear, which could be attributed to the typical disordered band (D band) and the graphene band (G band) of carbon, respectively [28-30]. The result of raman spectra indicates that the existence of CNTs, which is agree with above results.

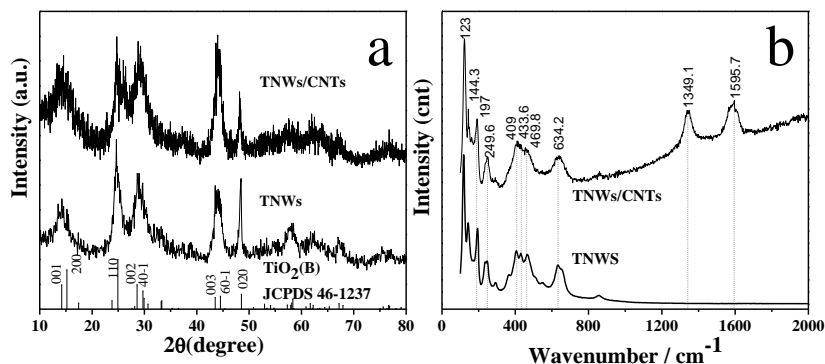


**Figure 2.** XRD patterns (a) and Raman spectra (b) of TNWs/CNTs and pure TNWs.

The present TNWs/CNTs feature a favorable microstructure and composition, which are attractive for addressing the existing issues for  $\text{TiO}_2$  as anodes of LIBs. We systematically investigated the electrochemical performance of synthesized TNWs/CNTs nanocomposites. The galvanostatic charge/discharge techniques were applied to study and compare the electrochemical properties of lithium insertion/extraction in half-cells based on TNWs and TNWs/CNTs respectively. Fig. 3a,b show the first discharge voltage profiles of samples at different current rates; and Fig. 3c,d show the cycling performance of samples at different current rates.

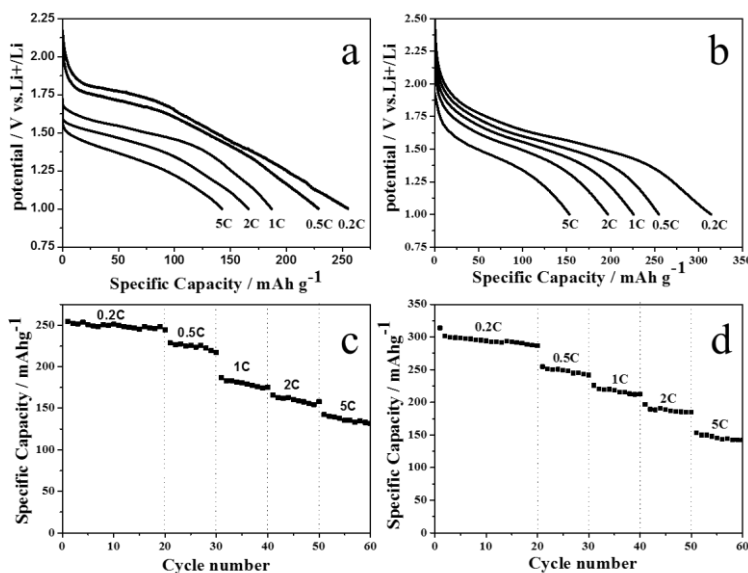


**Figure 3.** The first discharge voltage profiles of samples at different current rates: (a) pure TNWs; (b) TNWs/CNTs and cycling performance of samples at different current rates: (c) pure TNWs; (d) TNWs/CNTs.

Fig. 3a shows the first voltage profiles of pure  $\text{TiO}_2(\text{B})$  nanowires at different current rates respectively, there is no good flat discharge plateau. After adding CNTs, the nanocomposites demonstrate a better plateau, and the first discharge capacity reach to 314, 254.7, 226, 196.7 and 153.2  $\text{mAh}\cdot\text{g}^{-1}$  at 0.2, 0.5, 1, 2, 5C respectively (Fig. 3b), the cycling performance measurement shown in Fig. 3c,d also indicate that the TNWs/CNTs nanocomposites have higher specific capacity and better cycling stability than the pure TNWs. CNTs twining round TNBs surface play the role of ‘bridge’,

which will improve the Li ion and electron conductivity, on the other hand, the twining CNTs can improve the dispersion of nanocomposites, which will increase the electrolyte/electrode contact area and facilitate transportation of the electrolyte ion/electron into the inner region of the electrode. So the addition of CNTs can enhance both the specific capacity and the cycle performance of TiO<sub>2</sub>(B) nanowires.

Fig.4 displays the cycling performance of pure TiO<sub>2</sub>(B) nanowires and TNWs/CNTs nanocomposites with 0.4 g CNTs addition at 0.2 C. The specific capacities of TNWs and TNWs/CNTs are 234.8 and 343.92 mAh.g<sup>-1</sup> in the first cycle, respectively. After 200 charge/discharge cycles, they remained at 218.58 mAh.g<sup>-1</sup> (93% of initial discharge capacity) and 330.18 mAh.g<sup>-1</sup> (96% of initial discharge capacity), respectively. The TNWs/CNTs composites demonstrate a much higher specific capacity than pure TNWs and some other TiO<sub>2</sub>(B) nanostructures [24,26,27]. Especially, TNWs/CNTs demonstrate a good stability, which can be attributed to the enhanced electronic conductivity and improved dispersion gained from CNTs.

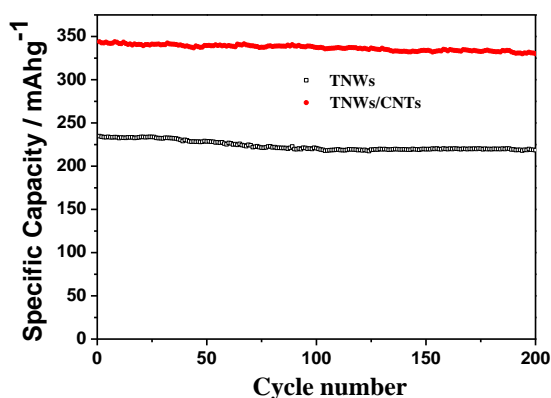
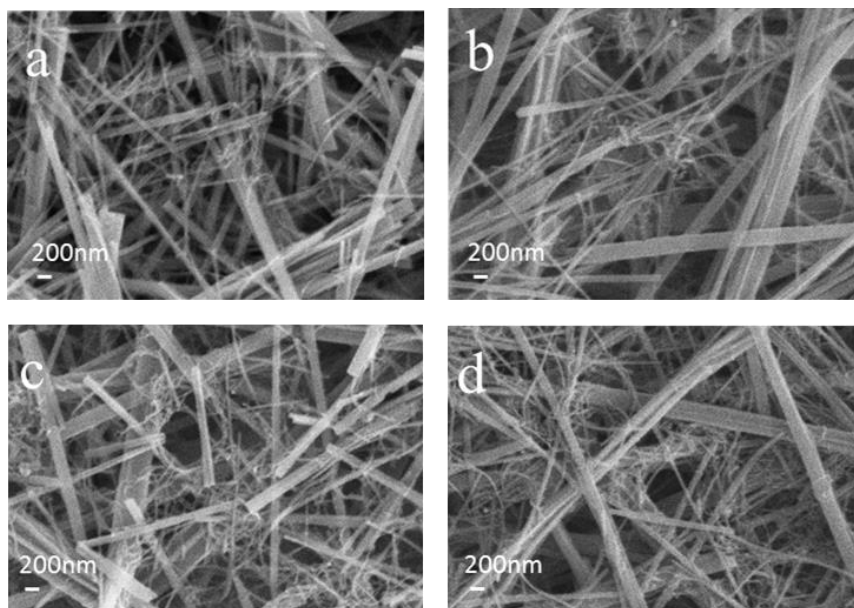


**Figure 4.** Cycling performance of pure TNWs and TNWs/CNTs at 0.2C rate

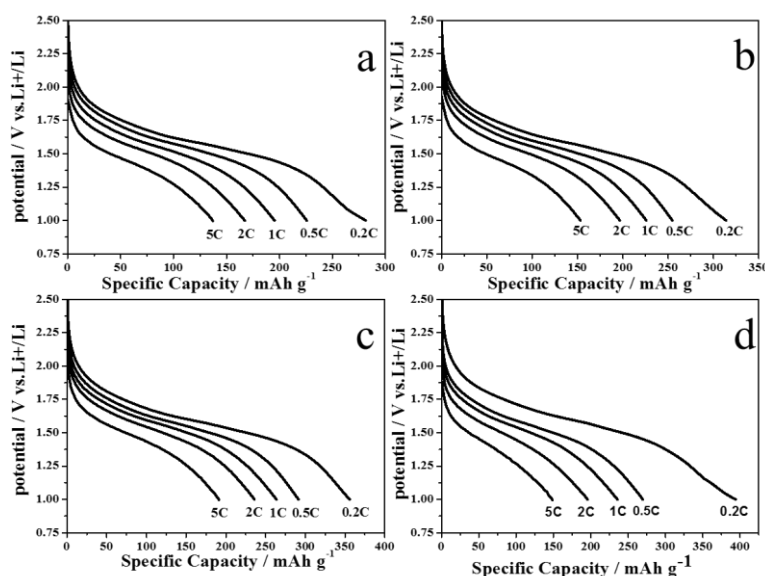
In order to investigate the effects of the CNTs on the TiO<sub>2</sub>(B) nanowires, we also compared the microstructures and performance of TNWs/CNTs nanocomposite with different CNTs addition. Fig. 5 shows the SEM images of TNWs/CNTs nanocomposites synthesized in the presence of 0.2, 0.3, 0.4 and 0.5 g CNTs respectively. Obviously, with the increasing carbon addition, more CNTs twine around the surface of TiO<sub>2</sub>(B) nanowires.

Fig. 6 displays the first discharge voltage profiles of TNWs/CNTs nanocomposites with different carbon content. When 0.2 g CNTs were added (Fig. 6a), the discharge capacities are 281.3, 225.7, 195.3, 175.1 and 136.9 mAh.g<sup>-1</sup> at 0.2, 0.5, 1, 2 and 5 C respectively. When CNTs content was 0.3 g, the discharge capacities increase to 314, 254.7, 226, 196.7 and 153.2 mAh.g<sup>-1</sup>, respectively (Fig. 6b). As the CNTs content was increased to 0.4 g, the TNWs/CNTs nanocomposites demonstrate a capacity of 355.9, 291.4, 263.8, 235.7 and 191.3 mAh.g<sup>-1</sup> at 0.2, 0.5, 1, 2 and 5 C respectively. The first discharge voltage profiles of TNWs/CNTs nanocomposites with 0.5 g CNTs addition is shown in Fig. 6d, its capacity continue increase to 393.9 at 0.2 C, but at higher current rate, the capacity become worse than that of 0.4 g CNTs sample, and it decreases to 269.5, 235.7, 195.5 and 148.9 mAh.g<sup>-1</sup> at 0.5, 1, 2 and 5 C rate respective. It indicates that carbon nanotubes can improve the performance of

lithium-ion battery, but there is a certain limit, when the carbon content is more than a certain range, it may actually reduce the performance.



**Figure 5.** The SEM images of samples with different CNTs addition (a) 0.2g; (b) 0.3g; (c) 0.4g; (d) 0.5g



**Figure 6.** The first discharge voltage profiles of samples with different carbon content: (a)0.2g; (b)0.3g; (c)0.4g; (d)0.5g

Fig. 7 compares the cycling performance at different rate among samples with different CNTs content. There is a capacity degradation phenomenon for all the samples accompanying increasing rates. When discharged at 0.2 C, the TNWs/CNTs-0.2 (with 0.2 g CNTs addition) demonstrates capacities of 281.3 mAh/g for the first cycle, 274.8 mAh.g<sup>-1</sup> for the second cycle and the irreversible capacity is 6.5

$\text{mAh}\cdot\text{g}^{-1}$ ; and the TNWs/CNTs-0.3, TNWs/CNTs-0.4 and TNWs/CNTs-0.5 electrode demonstrate the irreversible capacity of 12, 19.3 and  $42.7 \text{ mAh}\cdot\text{g}^{-1}$ , respectively. With the increase of carbon content, the irreversible capacity between the first and second discharge increased. The capacity loss could be attributed to the solid electrolyte interface (SEI) film. The SEI film are easy to form in carbon materials due to the reaction between electrolyte and carbon [31-33], the high surface area of CNTs affects the extent of solvent decomposition leading to the SEI formation [34,35], more CNTs induce more capacity loss, and then bigger irreversible capacity. Leaving out the first cycle, when discharged at 0.2 C for 19 cycles, TNWs/CNTs-0.2, TNWs/CNTs-0.3, TNWs/CNTs-0.4 and TNWs/CNTs-0.5 electrode possess capacities of 264.6, 286.6, 318.1 and 318  $\text{mAh}\cdot\text{g}^{-1}$  respectively, and their capacity retention ratios are 96.3%, 94.9%, 94.5% and 90.5% respectively. This indicates that in a certain CNTs range ( $<0.4\text{g}$ ), the capacity will increases significantly, and the cycling stability of the nanocomposite will become worse slightly. The TNWs/CNTs nanocomposites with 0.4 g CNTs addition have the highest specific capacity and excellent cycling performance. More CNTs ( $>0.4\text{g}$ ) will induce lower specific capacity, and worse cycling stability. When discharged at higher rate, this degradation phenomenon of specific capacity become more serious, at 5 C, the specific capacity are 143.8, 153.2, 191.3 and  $148.7 \text{ mAh}\cdot\text{g}^{-1}$  for TNWs/CNTs nanocomposites with 0.2, 0.3, 0.4 and 0.5 g CNTs addition respectively.

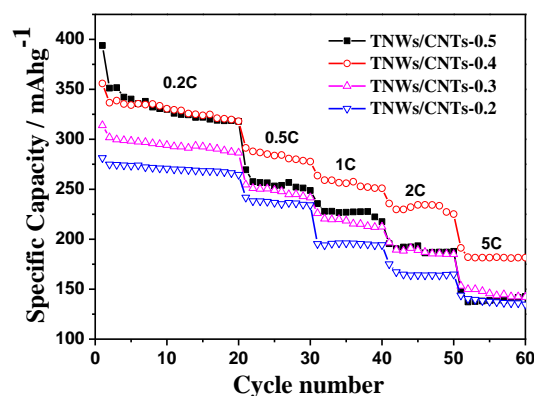


**Figure 7.** Cycling performance of samples at different current rates

#### 4. CONCLUSIONS

We have developed a facile route to synthesize TNWs/CNTs nanocomposites, which can be used as an advanced anode material for LIBs. The CNTs are twining around  $\text{TiO}_2(\text{B})$  nanowires, which serve as the ideal host for fast and efficient lithium storage. The addition of CNTs increased the specific surface area of the nanocomposites, and the contact area between the electrode material and the electrolyte, such structure is beneficial to lithium-ion insertion/extraction. Its specific capacity can reach to  $355.9 \text{ mAh}\cdot\text{g}^{-1}$  at 0.2C and  $191.3 \text{ mAh}\cdot\text{g}^{-1}$  at 5C, the capacity retention ratio is up to 90%.

#### ACKNOWLEDGMENTS

The authors gratefully acknowledge the financial support provided by the National Natural Science Foundation of China (No. 50872084, 51072124) and the Program for New Century Excellent Talents

in University (No. NCET100605). We wish to thank the Analytical & Testing of Sichuan University (SCU) for the assistance in sample characterization.

## References

1. J. Cabana, L. Monconduit, D. Larcher, M.R. Palacín. *Adv. Mater.*, 22 (35) (2010) E170–E192.
2. Y. Idota, T. Kubota, A. Matsufuji, Y. Maekawa, T. Miyasaka. *Science*, 276 (5317) (1997) 1395–1397.
3. X. Cao, Y. Shi, W. Shi, X. Rui, Q. Yan, J. Kong, H. Zhang. *Small*, 9 (20) (2013) 3433–3438.
4. Y.S. Hu, L. Kienle, Y.G. Guo, J. Maier. *Adv. Mater.*, 18 (11) (2006) 1421–1426.
5. Q. Wang, Z. Wen, J. Li. *Inorg. Chem.*, 45 (17) (2006) 6944–6949.
6. P.G. Bruce, B. Scrosati, J.M. Tarascon. *Angew. Chem. Int. Edit.*, 47 (16) (2008) 2930–2946.
7. H. Xiong, H. Yildirim, E.V. Shevchenko. *J. Phys. Chem.*, 116 (4) (2012) 3181–3187.
8. J.S. Chen, Y.L. Tan, C.M. Li. *J. Am. Chem. Soc.*, 132 (17) (2010) 6124–6130.
9. S.W. Kim, T.H. Han, J. Kim. *ACS nano*, 3 (5) (2009) 1085–1090.
10. H.G. Jung, S.W. Oh, J. Ce, N. Jayaprakash, Y. Sun. *Electrochem. Commun.*, 11 (4) (2009) 756–759.
11. H. Qiao, Y. Wang, L. Xiao, L. Zhang. *Electrochem. Commun.*, 10 (9) (2008) 1280–1283.
12. J. Ye, W. Liu, J. Cai, S. Chen, X. Zhao, H. Zhou, L. Qi. *J. Am. Chem. Soc.*, 133 (4) (2010) 933–940.
13. Y. Li, Z.Y. Fu, B.L. Su. *Adv. Funct. Mater.*, 22 (22) (2012) 4634–4667.
14. P. Kubiak, M. Pfanzelt, J. Geserick, N. Hüsing, U. Kaiserc, M. Wohlfahrt-Mehrensa. *J. Power Sources*, 194 (2) (2009) 1099–1104.
15. Y. Wang, X. Su, S. Lu. *J. Mater. Chem.*, 22 (5) (2012) 1969–1976.
16. J.Y. Shin, D. Samuelis, J. Maier. *Adv. Funct. Mater.*, 21 (18) (2011) 3464–3472.
17. Z. Wen, S. Ci, S. Mao, S. Cui, Z. He, J. Chen. *Nanoscale res. Lett.*, 8 (1) (2013) 1–6.
18. Z. Yang, G. Du, Q. Meng, Z. Guo, X. Yu, Z. Chen, T. Guo, R. Zeng. *J. Mater. Chem.*, 22 (12) (2012) 5848–5854.
19. F.F. Cao, X.L. Wu, S. Xin, Y.G. Guo, L.J. Wan. *J. Phys. Chem.*, 114 (22) (2010) 10308–10313.
20. L. Shen, X. Zhang, H. Li, C. Yuan, G. Cao. *J. Phys. Chem. Lett.*, 2 (24) (2011) 3096–3101.
21. J. Cai, Y. Wang, Y. Zhu, M. Wu, H. Zhang, X. Li, Z. Jiang, M. Meng. *ACS Appl. Mater. Inter.*, 7 (45) (2015) 24987–24992.
22. L. Zhang, D. Jing, X. She, H. Liu, D. Yang, Y. Lu, J. Li, Z. Zheng, L. Guo. *J. Mater. Chem.*, 2 (7) (2014) 2071–2078.
23. S.C. Zhang, D.J. Yang, D. Jing, H. Liu, L. Liu, Y. Jia, M. Gao, L. Guo, Z. Huo. *Nano. Res.*, 7 (11) (2014) 1659–1669.
24. Z. Zhang, Z. Zhou, S. Nie, H. Wang, H. Peng, G. Li, K. Chen. *J. Power Sources*, 267 (4) (2014) 388–393.
25. X. Zhu, X. Yang, C. Lv, S. Guo, J. Li, Z. Zheng, H. Zhu, D. Yang. *ACS Appl. Mater. Inter.*, 8 (2016) 18815–18821.
26. X. Yan, Y. Zhang, K. Zhu, Y. Gao, D. Zhang, G. Chen, C. Wang, Y. Wei. *J. Power Sources*, 246 (2014) 95–102.
27. H. Liu, Z. Bi, X.G. Sun, R.R. Unocic, M.P. Paranthaman, S. Dai, G.M. Brown. *Adv. Mater.*, 23 (30) (2011) 3450–3454.
28. X. Zhang, Z. Xing, L. Wang, Y. Zhu, Q. Li, J. Liang, Y. Yu, T. Huang, K. Tang, Y. Qian, X. Shen. *J. Mater. Chem.*, 22 (34) (2012) 17864–17869.
29. W. Zhu, H. Yang, W. Zhang, H. Huang, X. Tao, Y. Xia, Y. Gan, X. Guo. *RSC Adv.*, 5 (91) (2015) 74774–74782.
30. W. Zhou, Y. Liu, Y. Zhang, G. Yang, S. Deng, F. Shen, H. Peng, L. Wang. *New J. Chem.*, 38 (4)

- (2014) 1647-1654.
31. Y. Zhang, T. Chen, J. Wang, G. Min, L. Pan, Z. Song, Z. Sun, W. Zhou, J. Zhang. *Appl. Sur. Sci.*, 258 (10) (2012) 4729-4732.
  32. K. Kwon, F. Kong, F. Mclarnon, J.W. Evans. *J. Electrochem. Soc.*, 150 (150) (2002) A229-A233.
  33. J.R. Dahn, T. Zheng, Y. Liu, J.S. Xue. *Science*, 270 (5236) (1995) 590-593.
  34. B.J. Landi, M.J. Ganter, C.M. Schauerman, C.D. Cress, R.P. Raffaele. *J. Phys. Chem.*, 112 (19) (2008) 7509-7515.
  35. E. Frackowiak, F. Béguin. *Carbon*, 40 (10) (2002) 1775-1787.

© 2016 The Authors. Published by ESG ([www.electrochemsci.org](http://www.electrochemsci.org)). This article is an open access article distributed under the terms and conditions of the Creative Commons Attribution license (<http://creativecommons.org/licenses/by/4.0/>).